AIAA JOURNAL
Vol. 36, No. 6, June 1998

Modeling of Spatial Wind–Wave Correlations

Bård Venås* and Lars R. Sætran†
Norwegian University of Science and Technology, Trondheim N-7034, Norway
and
John B. Fossdal‡
Kongsberg Aerospace, Kongsberg N-3601, Norway

Wind-tunnel measurements of three components of mean wind and turbulence quantities, above a rigid three-dimensional realization of ocean waves, are reported. Based on the measurements a model is proposed for the cross correlations between wind fluctuations and the wave surface, including phase relations between the different components. The experiments are novel in the sense that spatial correlations are measured above a realistic multicomponent ocean-like wave surface, defined through its energy spectrum. The relevance of the model to flows above moving water waves are discussed through comparisons with other experimental results, for both moving and stationary waves.

Nomenclature

c	= wave velocity, m/s
$\mathcal{F}\{\}$	= Fourier transform
H	= wave height for harmonic surface, 2 × amplitude
H_s	= significant wave height, $4\sigma_h$
$h(x, y, t)$	= wave elevation, m
(k_x, k_y)	= wave numbers in the x–y plane, rad/m
k_0	= surface elevation wave number $2\pi/L$, rad/m
L	= mean wavelength, m
$Q_{\alpha\beta}(\Delta\xi)$	= correlation function, $R_{\alpha\beta}/\sigma_\alpha\sigma_\beta$
$R_{\alpha\beta}(\Delta\xi)$	= correlation between processes α and β, $[\alpha(\xi) - \overline{\alpha(\xi)}][\beta(\xi + \Delta\xi) - \overline{\beta(\xi)}]$
$S_{\alpha\beta}$	= cross spectrum, $\mathcal{F}\{R_{\alpha\beta}\}$
T	= wave period, s
t	= time, s
$\hat{\boldsymbol{U}}(\boldsymbol{x})$	= Reynolds-averaged mean velocity, m/s
$U(z)$	= mean velocity (horizontally averaged), m/s
$\boldsymbol{u} = [u, v, w]$	= wind velocities in Cartesian coordinates $\boldsymbol{x}$, m/s
$\hat{\boldsymbol{u}}'(\boldsymbol{x}, t)$	= Reynolds-averaged wind fluctuation, m/s
$\boldsymbol{u}'(\boldsymbol{x}, t)$	= wind fluctuation, m/s
$\boldsymbol{u}_w(\boldsymbol{x})$	= wave-induced wind fluctuation, m/s
$\boldsymbol{x} = [x, y, z]$	= Cartesian coordinates: x in streamwise direction, y in the transverse direction, and z in vertical direction, m
σ_α	= standard deviation of α, $\sigma_\alpha = \sqrt{(\overline{\alpha\alpha})}$

Introduction

SEVERAL experiments have reported wind fluctuations in the atmospheric ocean surface layer (typical heights $z < 50$ m) (Ref. 1), which are due to direct interaction between surface waves and wind. Most of these experiments report turbulence spectra or correlations as measured from instrumented platforms offshore or laboratory wind–wave facilities, where wave-induced fluctuations are found as additional peaks in the wind spectra (or equivalently periodicity in correlations) in bands around the wave frequency.[2–5] This is shown schematically in Fig. 1. The fluctuations are primarily reported in the streamwise u and the vertical w velocity, but results of Elder et al.[6] have indicated that similar fluctuations may also be present in the transverse direction (i.e., in the v component). The experiments referred to here primarily investigated momentum transfer across the ocean–atmosphere interface, for modeling purposes, and focused on changes in Reynolds' stresses, mean velocity profile, and transport of scalars such as temperature and humidity brought forward by the wind–wave interaction.

The starting objective for our work, however, was the modeling of wind structure close to wave surfaces for use in evaluation of wind impact on sea-skimming missiles. A preliminary investigation with a similar ambition had previously been reported by Lesieutre et al.,[7] who used a simple harmonic estimate for the periodicity of wave-induced fluctuations as input to missile flight simulations. They showed that a missile at transonic, or future supersonic, velocities may experience control problems due to such fluctuations when flying close to the sea surface. The important issue in this context is the possible occurrence of narrow-banded accelerations, caused by fluctuations in angles of attack or airspeed, which may alter the flight path, put critical strain on the airframe structure, or interact adversely with control system dynamics.

Figure 2 shows a simple conceptual model of streamlines above a wave surface being perturbed by the wave surface. If we accept this as a plausible model, it seems likely that a stationary measuring station will experience increased horizontal wind speed every time a wave passes the station due to acceleration over the wave crest. The wave period T will determine the frequency at which these fluctuations occur and thus the location of the wave peak in the spectrum. When looking at missiles traversing the air above waves, the main focus will be on the spatial rather than the temporal structure of the flow because the flight velocity is at least an order of magnitude higher than the velocity scales of the wind, justifying a view of the wind field as frozen, in the sense of Taylor's hypothesis for turbulent flows. The fluctuation frequencies that the missile experiences will therefore be determined by the surface wavelengths and the flight velocity.

This paper reports results from wind-tunnel measurements of three components of mean wind and turbulence quantities above a rigid three-dimensional realization of realistic ocean waves. The background for the experiment was, as described earlier, the desire to model spatial flow structures above natural waves. The surface was chosen to be able to describe wind–wave correlations in both horizontal directions, i.e., including the crosswind direction. The experiments and the model are believed to be novel approaches in analyzing spatial correlations above a realistic multicomponent wave surface. In addition to describing the experiment and deriving the model, this paper discusses the relevance to flows above moving water waves through comparisons with reported experimental results from offshore measurements, laboratory wind–wave facilities, and wind-tunnel flows above rigid two-dimensional waves.

The correlation model that is described in the paper has been implemented in a Monte Carlo turbulence simulation scheme, which has been described by Venås and Sætran.[8] In these simulations, numerically realized turbulence is added to realizations of wave-

Presented as Paper 97-0638 at the AIAA 35th Aerospace Sciences Meeting, Reno, NV, Jan. 6–9, 1997; received Feb. 5, 1997; revision received Jan. 30, 1998; accepted for publication Feb. 3, 1998.

*Ph.D. Student, Department of Mechanics, Thermo, and Fluid Dynamics.
†Associate Professor, Department of Mechanics, Thermo, and Fluid Dynamics. Member AIAA.
‡Senior Project Engineer, New Anti-Ship Missiles. Member AIAA.

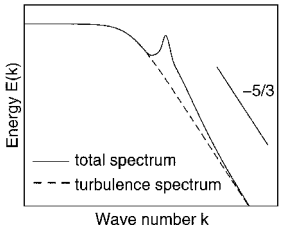

Fig. 1 Total wind spectrum as sum of a turbulence spectrum and a much narrower wave-induced wind spectrum (both axes are logarithmic).

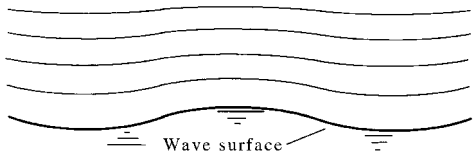

Fig. 2 Conceptual model: streamlines above wave surface.

induced fluctuations to provide realistic wind velocity time series for use in simulations of missile flight at low altitudes over waves.

Experiments on Wind–Wave Interaction

An actual ocean wave surface and its interaction with wind is a very complex process. First of all, the wave surface is highly three dimensional; i.e., it is not a monotonic wave train as sketched in Fig. 2. On the contrary, it consists of a continuous band of frequencies making a spectral description necessary. The wave velocity is not one distinct velocity because each wave component (harmonic) travels at a velocity proportional to its own wavelength and also spreads into directions other than that of the main wave propagation.[9] To complicate the situation even further, the wind does not have to be in equilibrium with the waves. This means that, as waves generate and dissipate slower than rapid changes in atmospheric wind, the main wave propagation may take place in any direction relative to the wind, e.g., in the direct opposite direction, as in Ref. 10.

Existing experimental studies of boundary-layer flows over waves seem to be divided into three separate approaches: actual offshore measurements, experiments in laboratory wind–wave facilities, and wind-tunnel experiments using rigid harmonic surfaces. Of these approaches offshore experiments have the obvious advantage of realistic wave surfaces and wind conditions. However, they suffer the same weakness as any full-scale atmospheric experiment: uncontrollable boundary conditions and difficult and expensive instrumentation. As far as is known to the authors, all offshore experiments have been limited to wind measurements at one horizontal position (x, y) as a function of height z and usually the wave elevation $h(x, y)$ at the same position. To provide accurate spatial information, however, one should measure spatial correlations directly (for example, by using a grid of wave elevation gauges and/or anemometers in the x–y plane) because the wave surface deforms over time due to the span of propagation velocities and the directional spreading.

Laboratory wind–wave experiments are controllable but have been limited to simple (mechanically generated) harmonic waves because available fetch is too small to develop wind-waves in laboratory scale. However, when using a harmonic wave surface, spatial correlations are available directly through phase averages because the waves propagate at one single velocity.

Rigid surfaces also provide both controllable surface conditions and easy access to phase-averaged measurements. The direct parallel to liquid wave surfaces may, however, be questioned due to the stationary no-slip boundary condition at the wall. The drift velocity of the waves (the mean motion of the water surface particles) is probably negligible compared with the wind and wave velocities, being on the order of 3% of U_{10}.[9] The wave propagation velocity on the other hand is likely to play a significant role in wind–wave interaction because it is the most dominant velocity scale of the water surface, usually being of the same order of magnitude as the mean wind velocity.

An elegant experiment investigating the effect of wave propagation was performed by Kendall,[11] who replaced a part of the wind-tunnel floor with a smooth neoprene rubber sheet, which could be mechanically deformed into progressive surface waves. In this way the ratio between wave velocity c and wind velocity U was varied continuously in the range $c/U \in \langle -0.5,\ 0.5 \rangle$ (i.e., with waves moving upwind, stationary waves, and waves moving downwind). Looking at the results, the rigid floor situation, $c/U = 0$, is not a singular point but a well-defined value along continuous curves for the different wind perturbation quantities as functions of c/U.

Based on this, and to investigate spatial correlations of wave-induced perturbations, we chose a somewhat different approach than the aforementioned ones: a wind-tunnel test above a rigid multicomponent three-dimensional wave surface. A rigid surface has evidently zero wave velocity, which again, of course, is not physically viable. But as was pointed out earlier, wave propagation in the ocean may have any direction other than that of the mean wind, and the stationary wave situation may thus be considered an intermediate value of the c/U ratio. Advantages in using a rigid surface are the easy access to spatial correlations and the freedom in choice of surface topography. This last point meant that we had the possibility of testing developed wind–waves in the laboratory by creating a wave surface in accordance with established results for ocean waves. The results presented here should, however, be considered in the light of the restraint that the zero c/U value may put on its applicability. Aspects of this are discussed further later in the paper.

Experimental Details

The utilized wave surface was made as a Gaussian realization of the Joint North Sea Wave Project (JONSWAP) spectrum for partially developed wind–waves, using the directional spectrum of Hasselmann et al.[12] for transforming it into a two-dimensional spatial spectrum, i.e., from $S_{hh}(\omega)$ to $S_{hh}(k_x, k_y)$. The realization of the spectrum was performed numerically and used directly as input to a digital plain milling machine. The surface and a cut along the centerline of the model are shown in Fig. 3.

The experiments were conducted in a $11.2 \times 2.7 \times 1.8$ m^3 (length $\times$ width $\times$ height) wind tunnel. The wave model had a dimension 7×2.6 m with a mean wavelength $L = 1200$ mm and a maximum difference in surface elevation of 100 mm (lowest through to highest crest). The choice of these scales was based on a compromise between the desire for a large number of wave events and a good experimental resolution. Further, the steepness of waves are usually defined through the ratio between the wave height H_s and the wavelength L, and the wave surface spectrum was scaled to get an H_s/L ratio corresponding to normal but still quite choppy seas; $H_s = 59$ mm gave an H_s/L ratio of roughly 0.05, complying with this specification. The surface can therfore be perceived as a typical, extreme, nonbreaking wave surface in approximately 1:100 scale, which has been frozen in time.

A thick turbulent boundary-layer/shear flow was set up by placing spires at the entrance to the test section in accordance with the method of Counihan[13] for simulating neutral atmospheric boundary layers. This was done to create a fully turbulent situation over the short distance upstream of the waves. Because the mean surface level of the model is located above the wind-tunnel floor, the floor was raised to this new zero level (65 mm) just after the spires. The wind-tunnel configuration is shown schematically in Fig. 4.

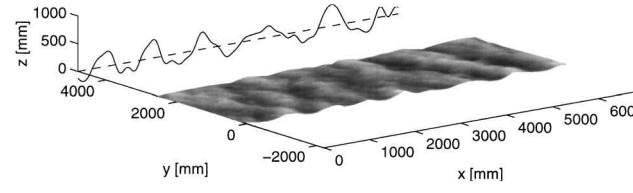

Fig. 3 Wave model topography (not in scale); back: cut along the centerline of the model (multiplied 10 times).

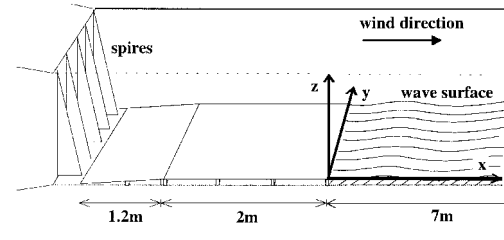

Fig. 4 Wind-tunnel test section configuration.

Constant temperature hot-wire anemometry was employed for measuring mean wind and fluctuating turbulence quantities along the model. To speed up the data acquisition and to get an estimate of the spatial turbulence correlations along the model, two x-wire probes were used simultaneously, with an internal separation of $\Delta y = 100$ mm. The flow was allowed to pass the first two waves before reaching the foremost measuring location at $x = 2200$ mm. Measurements were performed in four horizontal planes: $z = 55$, 100, 150, and 300 mm above the mean surface level. In each of the planes the probes were traversed in rectangular grids of 21×16 points ($\Delta x = 200$ mm and $\Delta y = 100$ mm). Two series of measurements were conducted: with the hot wires oriented in the vertical plane and with the wires in the horizontal plane, for measuring u-w and u-v quantities, respectively.[14]

Definition of the Problem

The results analysis is based on a triple decomposition of the instantaneous wind velocity, adding the term wave-induced wind fluctuation $\boldsymbol{u}_w$ to the standard Reynolds decomposition

$$\boldsymbol{u} = \boldsymbol{U} + \boldsymbol{u}' + \boldsymbol{u}_w = U + [u', v', w'] + [u_w, v_w, w_w] \tag{1}$$

where the rules of Reynolds decomposition apply to both types of fluctuations ($\bar{u}' = \bar{v}' = \bar{w}' = \bar{u}_w = \bar{v}_w = \bar{w}_w = 0$) and the coordinate system x axis is oriented along the mean wind direction ($\boldsymbol{U} = [U, 0, 0]$).

It is, however, not self-evident what the different fluctuations describe physically. Kitaigorodskii[2] defines wave influence as wave perturbations in the turbulence field above the surface, whereas turbulent fluctuations are said to be turbulence of purely atmospheric origin. We have used a slightly different definition, stating that the wave perturbation is the part of the fluctuations that correlates with the ocean surface elevation, i.e.,

$$\boldsymbol{u}_w(\boldsymbol{x}, t) = \boldsymbol{u}_w[h(x, y, t), z, U] \tag{2}$$

meaning that $\boldsymbol{u}_w$ is a deterministic rather than a stochastic function of the surface elevation h. Thus, the randomness of the wave-induced fluctuations is a result of the stochastic nature of the waves. In Eq. (2) we have further assumed that $\boldsymbol{u}_w$ is a function of height z and scales on the mean velocity U.

The turbulence component $\boldsymbol{u}'$, on the other hand, is defined as the part of the fluctuations that does not correlate with h:

$$R_{\boldsymbol{u}'h}(\Delta x, \Delta y, z, \Delta t) = \overline{\boldsymbol{u}'(\boldsymbol{x}, t) h(x + \Delta x, y + \Delta y, t + \Delta t)} \equiv 0 \tag{3}$$

though its stochastic nature may be a function of h. This is to say that other statistics of $\boldsymbol{u}'$, such as higher-order moments (e.g., $\sigma_{\boldsymbol{u}'}$), may be functions of h. This differs from Kitaigorodskii's definition in that he defines $\boldsymbol{u}_w$ as containing all correlations between $\boldsymbol{u}$ and h in the strict sense, whereas we only assume this for first-order statistics. As we will see later, the difference between the two definitions is probably not very significant in this experiment.

Our definition results in cross correlations between instantaneous velocity and surface elevation of the form

$$\begin{aligned} R_{\boldsymbol{u}h}(\Delta x, \Delta y, z, \Delta t) &= \overline{\boldsymbol{u}(\boldsymbol{x}, t) h(x + \Delta x, y + \Delta y, t + \Delta t)} \\ &= \overline{[\boldsymbol{U}(\boldsymbol{x}) + \boldsymbol{u}'(\boldsymbol{x}, t) + \boldsymbol{u}_w(\boldsymbol{x}, t)] h(x + \Delta x, y + \Delta y, t + \Delta t)} \\ &= \overline{\boldsymbol{u}_w(\boldsymbol{x}, t) h(x + \Delta x, y + \Delta y, t + \Delta t)} \\ &= R_{\boldsymbol{u}_w h}(\Delta x, \Delta y, z, \Delta t) \end{aligned} \tag{4}$$

which means that the cross correlation can be used for extracting the wave-induced velocities from the total signal.

To evaluate the data using these definitions, the measurements were first time averaged according to standard Reynolds decomposition, that is, into local mean velocities

$$\hat{\boldsymbol{U}}(\boldsymbol{x}) = \frac{1}{\tau} \int_0^\tau \boldsymbol{u}(\boldsymbol{x}, t)\, \mathrm{d}t \tag{5}$$

and zero-mean time series

$$\hat{\boldsymbol{u}}'(\boldsymbol{x}, t) = \boldsymbol{u}(\boldsymbol{x}, t) - \hat{\boldsymbol{U}}(\boldsymbol{x}) \tag{6}$$

From these the triple decomposition was evaluated as

$$\boldsymbol{U}(z) = \frac{1}{N_x N_y} \sum_{i=1}^{N_x} \sum_{j=1}^{N_y} \hat{\boldsymbol{U}}(x_i, y_j, z) \tag{7}$$

$$\boldsymbol{u}'(\boldsymbol{x}, t) = \hat{\boldsymbol{u}}'(\boldsymbol{x}, t) \tag{8}$$

$$\boldsymbol{u}_w(\boldsymbol{x}) = \hat{\boldsymbol{U}}(\boldsymbol{x}) - \boldsymbol{U}(z) \tag{9}$$

where (x_i, y_j) defines the measuring positions in each plane z. The overall mean velocity $\boldsymbol{U}$ equals the mean of $\hat{\boldsymbol{U}}$ in the x–y plane, and the wave influence is defined as the deviations in $\hat{\boldsymbol{U}}$ along the model. Because we here consider the flow above rigid waves, the surface elevation is not a function of time, and the same therefore applies for the wave-induced perturbations. Because of this, t is not present in the following analysis, although it should be for the general case.

For the preceding evaluation to be in accordance with the definitions of the triple decomposition, $\boldsymbol{u}_w$ should correlate fully with $h(x, y)$; that is, it should not have any other functional relationship with x or y than through h. Whether this is the case is discussed in the two next sections, in which we describe, respectively, the correlation between the wave surface and the flow and the modeling of it. A necessary but less strict consequence of the definition of $\boldsymbol{u}_w$ is that it should be homogeneous in the x–y plane. This is not per definition necessary for $\boldsymbol{u}'$ but should be satisfied anyway if the overall flow is to be considered homogeneous. To evaluate whether homogeneity is satisfied, Fig. 5 shows $\sigma_{u'}/U$ and u_w/U (both for $z = 100$ mm) as functions of x along the centerline of the model. In the figure we see that the turbulence level is fairly constant compared with the fluctuations in u_w. The turbulence autocorrelation function $Q_{u'u'}(x,\ \Delta y = z = 100$ mm, $\Delta t = 0)$ is also shown in the figure. We judge all of these results, both in turbulence level and in correlation level (an indication of the length scale), to be close to constant compared with the wave-induced fluctuations, indicating that u' may be considered as homogeneous.

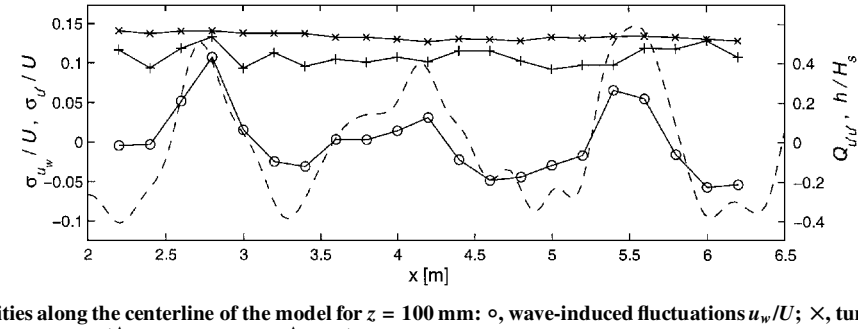

Fig. 5 Turbulence quantities along the centerline of the model for z = 100 mm: ∘, wave-induced fluctuations u_w/U; ×, turbulence intensity $\sigma_{u'}/U$; +, turbulence correlation function $Q_{u'u'}$ (Δy = 100 mm and Δt = 0); and - - -, wave surface elevation h/H_s.

Wave-Induced Correlations

Measured cross-correlation functions between the different components of $\boldsymbol{u}_w$ and the surface elevation h are shown in Fig. 6. The bottom figure shows the autocorrelation function Q_{hh} of the surface elevation in the same (i.e., the utilized) region of the model. The term Q_{hh} is the inverse Fourier transform of the JONSWAP spectrum $S_{hh}(k_x, k_y)$ and qualitatively has the character of an exponentially decaying cosine function in the x direction, the distance between the peaks being the mean wavelength L. In the y direction the function has approximately the same wave length but a much faster exponential decay, nearly suppressing all oscillations (the function is slightly negative for $\Delta y/L = 0.5$). The shape of the correlation tells that the surface is quite periodic in the x direction, as would be anticipated. In the y direction there is almost no periodicity but a fairly long correlation length, meaning that the waves have a significant width with respect to the wavelength. The nonideal and nonsymmetric form of Q_{hh} in Fig. 6 is due to the model realization being of limited size.

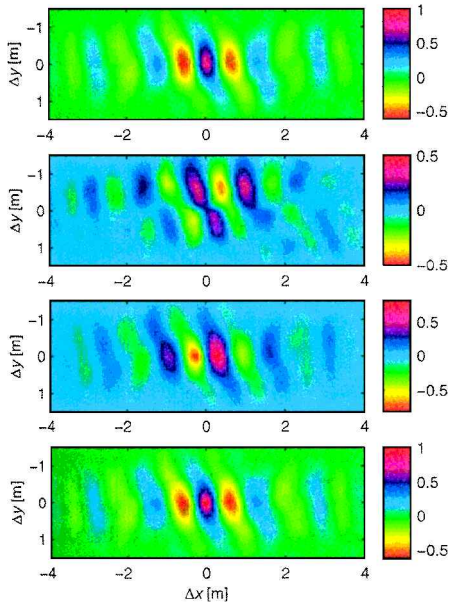

Fig. 6 Measured wave-induced fluctuations at $z = 100$ mm. From the top downward: $Q_{u_w h}$, $Q_{v_w h}$, and $Q_{w_w h}$. Bottom: corresponding autocorrelation function of wave elevation Q_{hh}.

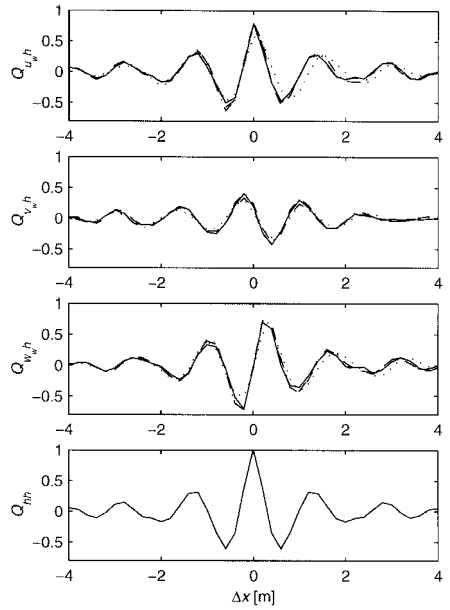

Fig. 7 From above: $Q_{u_w h}$, $Q_{v_w h}$, $Q_{w_w h}$, and Q_{hh} plotted along the x axis ($\Delta y = 0$) except for $Q_{v_w h}$, which is along $\Delta y = 500$ mm. The lines represent the different heights: —, $z = 55$ mm; - - -, $z = 100$ mm; –·–, $z = 150$ mm; and · · · ·, $z = 300$ mm.

The cross-correlation function $Q_{u_w h}$ resembles quite closely Q_{hh}, even having the same general trend of being slightly skewed counterclockwise. The perturbations are close to exactly in phase with the surface elevation and have the same form of exponentially decaying oscillations in the x direction. The exact match in value is not found in the origin where $Q_{u_w h} = 0.81$ and thus does not correspond fully to the default autocorrelation value $Q_{hh} = 1$. For all other separations $(\Delta x, \Delta y)$, however, the two correlation coefficients seem equal within reasonable accuracy. This can easily be seen in Fig. 7, which shows cuts along the correlation surfaces for the different planes. Here we also notice that the same picture prevails for all values of z; that is, there seems to be little change with height within the measuring range.

The correlation function $Q_{w_w h}$ suggests that the vertical fluctuation lags the surface by approximately $\pi/2$. Because u_w was found to be in phase with the surface, this means that u_w leads w_w by $\pi/2$. By the expressions lead and lag here we mean the location along the x axis. This is also equal to the order of events in a situation where the waves move downwind past a stationary measuring station. The term $Q_{v_w h}$ seems to change phase depending on the sign of Δy. That this in fact should be the case can be reasoned from the fact

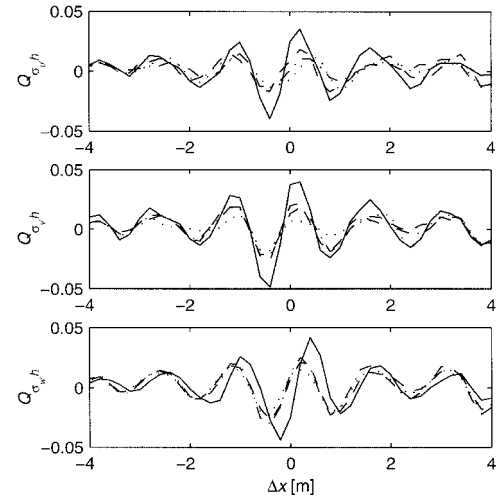

Fig. 8 Correlation between turbulence intensity (normalized by σ_{u_w} at $z = 100$ mm) and surface elevation. From top to bottom: $Q_{\sigma_{u'} h}$, $Q_{\sigma_{v'} h}$, and $Q_{\sigma_{w'} h}$. Note: all correlations are normalized by σ_{u_w} ($z = 100$ mm) for comparison with Figs. 6, 7, and 9; lines are as in Fig. 7.

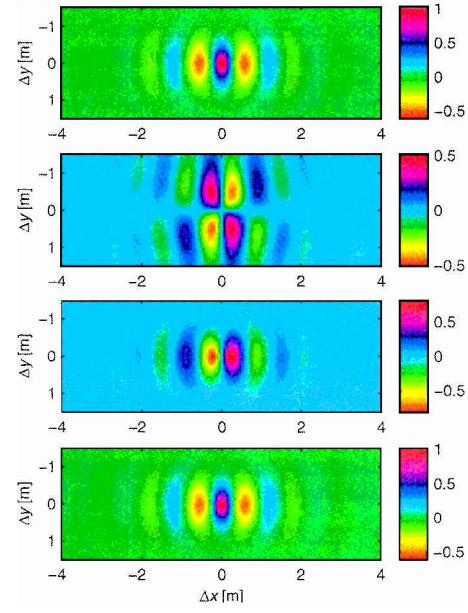

Fig. 9 Modeled correlation functions. From the top downward: $Q_{u_w h}$, $Q_{v_w h}$, and $Q_{w_w h}$. Bottom: autocorrelation functions of wave elevation Q_{hh}.

that the correlation in the mean has to be antisymmetric about the x axis because no direction can be favored. The reason why this is not evident from the measurements can be the fact that the absolute values of fluctuations are smaller in this component than in the two other components and that the aforementioned skewing of the surface may have masked the result to a certain extent.

In the preceding section the turbulence was shown to be close to homogeneous in the x–y plane. It is, though, slightly affected by the surface elevation as can be seen from Fig. 8, which shows cross correlations between the turbulence standard deviation (note, normalized by σ_{u_w} at $z = 100$ mm for comparison) at different heights and the wave surface elevation. Generally the turbulence leads the waves, although there is some difference between the components and changes with height. Using the Kitaigorodskii[2] definition of the triple decomposition (preceding section), this turbulence perturbation would have been included in the wave-induced perturbation part because it includes all wave perturbations of the flowfield. However, the magnitude of the turbulence–wave correlation is at the most only about 5% of the maximum wave-induced correlation, and so the two definitions do not differ very much in this case. As the values of the variations in turbulence intensity are small compared with the fluctuations in $\boldsymbol{u}_w$, they are not considered in the further modeling and discussion.

Modeling

As mentioned in the preceding text, $Q_{u_w h}$ resembles Q_{hh} quite closely, except near $\Delta x = \Delta y = 0$, where it has a slightly lower value. There may be at least two reasons for this: it may be an actual physical process that the lag or the strength of the wave-induced perturbation varies somewhat for the individual waves due to higher-order effects. It may also be caused by u_w not being fully homogeneous in our experiment: if the overall mean velocity had, for example, a downstream trend, such an inhomogeneity would enter into u_w (based on the evaluation of the triple decomposition). This again would increase the apparent standard deviation σ_{u_w}, downscaling the correlation function $Q_{u_w h}$. It is difficult to determine which of these (or whether both) factors play a role in our experiment due to the short measuring region. We have therefore modeled the correlation as

$$Q_{u_w h}(\Delta x, \Delta y, z) = Q_{hh}(\Delta x, \Delta y) \tag{10}$$

because this represents both a close approximation and a simple definition. The model then gives for the scaled cross correlation

$$R_{u_w h}(\Delta x, \Delta y, z) = \frac{\sigma_{u_w}(z)}{\sigma_h} R_{hh}(\Delta x, \Delta y) \tag{11}$$

The Fourier transform $\mathcal{F}\{\,\}$ of the cross correlation yields the cross spectrum

$$S_{u_w h}(k_x, k_y, z) = \frac{\sigma_{u_w}(z)}{\sigma_h} S_{hh}(k_x, k_y) \tag{12}$$

Figure 6 indicates a $\pi/2$ rad phase lag between the vertical and the streamwise fluctuations, a result also found in the offshore measurements of Antonia and Chambers.[3] They reported this to be "consistent with a description of the interaction between waves and turbulence as a quasi-potential wave perturbation of the turbulent flow." Continuing this line of thought, the potential flow solution for a two-dimensional, harmonic, and stationary wave surface, $h = (H/2)\sin(k_0 x)$, has the form (using linearized boundary conditions at the wave surface: $w_w|_{z=0} = U\mathrm{d}h/\mathrm{d}x$)

$$u_w = U(Hk_0/2)\sin(k_0 x)\exp(-k_0 z) \tag{13}$$

$$w_w = U(Hk_0/2)\cos(k_0 x)\exp(-k_0 z) \tag{14}$$

meaning that the horizontal and vertical fluctuations are $\pi/2$ rad out of phase. The cross-correlation functions between the perturbations and the wave surface are then

$$Q_{u_w h}(\Delta x) = \cos(k_0 \Delta x) \tag{15}$$

$$Q_{w_w h}(\Delta x) = \sin(k_0 \Delta x) \tag{16}$$

For a harmonic surface the sine-cosine relationship is represented simply through this $\pi/2$ phase lag. The result may, however, also be used to describe the differences between the $Q_{u_w h}$ and $Q_{w_w h}$ correlations found in our measurements, having, respectively, the form of a qualitatively decaying cosine and a similarly decaying sine along the x coordinate (Fig. 7). From the preceding equations, we find the following relationship between the two cross correlations:

$$\cos(k_0 \Delta x)\frac{R_{w_w h}(\Delta x)}{\sigma_{w_w}} = \sin(k_0 \Delta x)\frac{R_{u_w h}(\Delta x)}{\sigma_{u_w}} \tag{17}$$

The multiplication by trigonometric functions corresponds to shifting the spectra into side bands in Fourier space. In other words, the Fourier transform of Eq. (17) gives (e.g., see Ref. 15)

$$\frac{1}{2\sigma_{w_w}}\left[S_{w_w h}(k_x - k_0) + S_{w_w h}(k_x + k_0)\right] = \frac{1}{2\sigma_{u_w} i}\left[S_{u_w h}(k_x - k_0) - S_{u_w h}(k_x + k_0)\right] \tag{18}$$

an equation that has the obvious solution

$$S_{w_w h} = -\left(\sigma_{w_w}/\sigma_{u_w}\right) S_{u_w h}\,\mathrm{sgn}(k_x) i = \left(\sigma_{w_w}/\sigma_{u_w}\right) S_{u_w h}\exp[-(\pi/2)\,\mathrm{sgn}(k_x) i] \tag{19}$$

where $\mathrm{sgn}(k_x)$ is the signum function $\{\mathrm{sgn}(k_x) = [-1, 0, 1]$ for $k_x \in [<0, =0, >0]\}$. For the potential flow solution the cross spectra are thus equal in amplitude but differ in phase. Similarly, for a harmonic surface Eq. (19) represents the difference between a sine and a cosine, whereas for a multiple component spectrum the equation says that each individual wave component is shifted $\pi/2$ rad out of phase, i.e., one-fourth of its own proper wavelength.

A similar analysis can be performed for the crosswind component of the wave-induced fluctuation. If $Q_{v_w h}$ is assumed antisymmetric, in both the x and the y direction, we get

$$S_{v_w h} = -\left(\sigma_{v_w}/\sigma_{u_w}\right) S_{u_w h}[\mathrm{sgn}(k_x) - \mathrm{sgn}(k_y)] i = \left(\sigma_{v_w}/\sigma_{u_w}\right) S_{u_w h}\exp\{-(\pi/2)[\mathrm{sgn}(k_x) - \mathrm{sgn}(k_y)] i\} \tag{20}$$

The model cross-correlation functions are shown in Fig. 9 as they are evaluated from this modeling, that is, as the inverse Fourier transform of the cross spectra in Eqs. (12), (19), and (20). Compared with the measured results (Fig. 6), we see a good quantitative correspondence in all three components, considering that the measurements are performed over a relatively limited size realization of the wave spectrum.

Measured values of σ_{u_w}, σ_{v_w}, and σ_{w_w} are plotted in Fig. 10 (top) normalized by the local mean velocity $U(z)$. The wave-induced

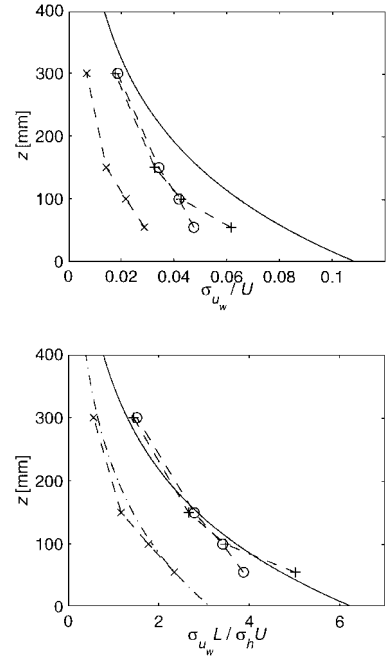

Fig. 10 Intensity of wave-induced fluctuations: ∘, u_w; ×, v_w; +, w_w; and ——, potential flow solution [–·–, potential flow value divided by 2; Eq. (27)] normalized by $U(z)$ (top) and by $\sigma_h U/L$ (bottom).

fluctuations are here seen to be close to equal in the streamwise and the vertical direction, as predicted by the potential flow solution. In the transverse direction, on the other hand, the perturbations have approximately half this value. The experiment of Elder et al.[6] is the only one known to us that has found transverse fluctuations over waves. One reason for this may be that the fluctuations are substantially weaker in this direction than in the others, as indicated by this result.

The wind-induced fluctuations decay almost exponentially with height. This corresponds well with the measurements of Frederick and Hanratty[16] over two-dimensional harmonic waves of approximately the same wave height to wavelength ratio. They report the wave-induced correlations to extend to a height equal to about half the wavelength ($L/2$, in our case $z = 600$ mm). Also plotted in Fig. 10 is the corresponding standard deviation based on the potential flow solution. We see an exponential decay with height but a somewhat higher fluctuation value. However, when normalizing by the standard deviation of the wave surface, as is shown in the lower plot of Fig. 10, a very close match is found. This result is a consequence of the difference between the standard deviation to wave height ratio of the modeled ocean wave surface and the sinusoidal surface

$$\sigma_{h,\text{sine}} = (H/2)\sqrt{\overline{\sin^2(k_0 x)}} = (H/2)\sqrt{1/2} \tag{21}$$

$$\sigma_{h,\text{ocean}} = (H_s/4) \tag{22}$$

where the ocean waves' value follows from the definition in the Nomenclature (see, for example, Ref. 9).

To incorporate the fluctuation levels in the model, we scale the cross spectra by the respective standard deviations

$$S_{u_w h}(k_x, k_y, z) = \frac{\sigma_{u_w}(z)}{\sigma_h} S_{hh}(k_x, k_y) \tag{23}$$

$$S_{v_w h}(k_x, k_y, z) = \frac{\sigma_{v_w}(z)}{\sigma_h} \exp\left\{-\frac{\pi}{2}[\text{sgn}(k_x) - \text{sgn}(k_y)]i\right\} S_{hh}(k_x, k_y) \tag{24}$$

$$S_{w_w h}(k_x, k_y, z) = \frac{\sigma_{w_w}(z)}{\sigma_h} \exp\left[-\frac{\pi}{2}\text{sgn}(k_x)i\right] S_{hh}(k_x, k_y) \tag{25}$$

where the standard deviations are modeled as

$$\sigma_{u_w}/\sigma_h = U k_0 \exp(-k_0 z) \tag{26}$$

$$\sigma_{v_w} = \sigma_{u_w}/2 \tag{27}$$

$$\sigma_{w_w} = \sigma_{u_w} \tag{28}$$

based on the experiments and the potential flow solution.

Discussion

The modeling in the preceding section stems from the result that the cross-correlation function between streamwise fluctuations and the wave elevation can be approximated as $Q_{u_w h} = Q_{hh}$. This is, in fact, the same as stating that the wave-induced fluctuation in the mean wind direction can be represented as a scaling of the surface elevation, i.e.,

$$u_w(x, y, z) = \frac{\sigma_{u_w}(z)}{\sigma_h} h(x, y) \tag{29}$$

as is the case for the potential flow solution. The analysis from Eq. (13) and on then follows from a two-dimensional approach. However, as can be seen in Figs. 6, 9, and 10, this seems to give good results also for the three-dimensional surface, leading to Eqs. (23–28). The whole model can be seen as a filtering of the surface elevation h through gain factors [Eqs. (26–28)] and phase shifting of the surface elevation spectrum S_{hh}. The frequency contents are equal to that of the wave surface, but the amplitude levels are scaled separately for the different fluctuations. Similarly, the phase spectrum changes drastically from the u_w to the v_w and w_w components.

The close resemblance to a potential flow indicates that the flow stays attached along the model wave surface. A visualization of this was performed by placing a number of free-moving tufts close to the surface. At all times, all tufts stayed close to or fluctuated only slightly about the downwind direction, meaning that no (neither mean nor intermittent) flow separation takes place. This is also in accordance with the results of Zilker and Hanratty[17]: the Reynolds numbers of our experiment, both viscous ($Re = u_* L/\nu \approx 10^4$) and mean flow based ($Re = UL/\nu \approx 5 \times 10^5$) are about two orders of magnitude higher than the high limit for separated flow that they list for a sinusoidal wave train with an H/L ratio of 0.05.

Both the experiment and the potential flow solution [Eqs. (13) and (14)] are for stationary wave surfaces, which is an unphysical situation for an air–water interface. However, it was earlier argued that this represents just another value of the ratio c/U. To study this more closely, we can allow for a wave velocity c in the potential solution

$$u_w = (U - c)(Hk_0/2)\sin[k_0(x - ct)]\exp(-k_0 z) \tag{30}$$

$$w_w = (U - c)(Hk_0/2)\cos[k_0(x - ct)]\exp(-k_0 z) \tag{31}$$

If the wind velocity is higher than the wave velocity ($U > c$), the horizontal fluctuation u_w will be in phase with the wave surface. If the wave velocity exceeds the wind speed ($c > U$), on the other hand, the sign of the perturbation will change and the fluctuation will be π rad out of phase. This can be viewed conceptually as if the surface, instead of perturbing a passing flow, sets up a motion by pumping the airflow, as is shown schematically in Fig. 11b.

Here, note that it is not our intention to provide sophisticated modeling of the fluid dynamic processes in the interfacial layer but to highlight the findings from our experiment with a complex and realistic ocean surface topography. A good starting point for modeling of airflow above waves and wind–wave interaction may, for instance, be the work of Mastenbroek et al.[5] or Belcher et al.,[18] who consider the two-dimensional Reynolds-averaged momentum and turbulence equations for, respectively, the flow above a wave surface and the coupling between the airflow and the flow in the water surface layer.

However, several experiments indicate that the results from the preceding general potential solution are at least qualitatively correct. Both Kendall[11] and Frederick and Hanratty[16] found streamwise velocity perturbations nearly in phase with the surface elevation for $c/U = 0$. The results vary slightly with distance from the wall, Reynolds number, wave steepness, etc., but well within reasonable limits, comparing the different experiments.

In Kendall's tests with the wave surface moving against the wind ($c/U \in [-0.5, 0\rangle$) the wall pressure is close to π rad out of phase, indicating that the velocity is in phase with the waves near the surface, as it is for the stationary surface (velocity is not measured directly for $c/U < 0$). This result also corresponds well with the offshore measurement of Kondo et al.,[10] who with near opposite directions of wind and wave propagation found in-phase correlation between the streamwise wind fluctuations and the surface elevation. The results of Mastenbroek et al.[5] from a laboratory wave flume similarly

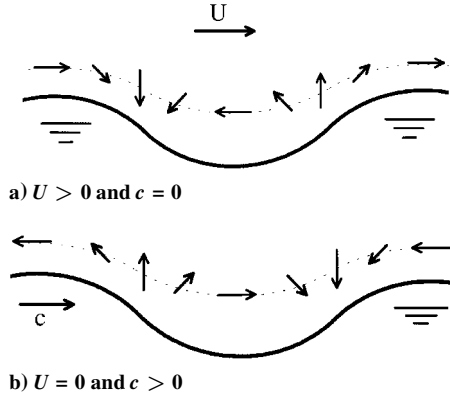

a) $U > 0$ and $c = 0$

b) $U = 0$ and $c > 0$

Fig. 11 Schematic of the direction of wave perturbations.

indicate little phase shift for $c/U = 0.25$, whereas the phase shift for $c/U = 0.55$ is difficult to determine due to the low signal-to-noise ratio (note: U_∞ in their paper is replaced by local velocity U). When c approaches U, the potential solution indicates that the fluctuations gradually fade away. In line with this, for $c/U \approx 1$, Kondo et al. report very low correlation between the wind and the waves and the fact that the phase relation becomes obscure. The magnitude of the fluctuations in Kendall's experiments is highest for the lowest value of c/U (-0.5) and decays with increasing c/U. When the wave velocity exceeds the wind velocity, Kondo et al. found near π rad phase shift as stated by the potential solution [Eqs. (30) and (31)].

As a conclusion, it seems that the qualitative results from the potential solution are close to what has been found experimentally when c is sufficiently different from U. When c is close to U, however, viscous and turbulence effects are likely to play increasingly important roles. Keeping this in mind, a first-order approximation to the general case can be achieved by combining Eqs. (26–28), (30), and (31), substituting Eq. (26) with

$$\sigma_{u_w}/\sigma_h = (U - c)k_0 \exp(-k_0 z) \tag{32}$$

in the model equations.

The model outlined in this paper thus represents a means for describing the spatial behavior of the flow when there is a significant difference between the wind and wave velocity. More experimental results should be compared with the model to check the validity of the predicted magnitude of $\boldsymbol{u}_w$. Further, the approximative analysis of phase shifts seems sufficient for flight simulations but not for providing insight into the generation of wind waves (for example, see Ref. 19). Here, small phase shifts are one of the causes creating drag on the waves, resulting in momentum transfer between wind and waves.

For situations in which there is not a clear separation between the wind and wave velocities, the temporal parameters, time t and wave velocity c, should be introduced to the analysis. Anyway, the fact that here a clear relationship has been found between the wave-induced perturbations and the spatial shape of the surface indicates that the spatial coordinates, if possible, should also remain in the analysis in situations where $c \approx U$, when a nonharmonic wave surface is to be described.

Conclusion

The experiments have resulted in a model for wave-induced wind fluctuations in all three velocity components. The model is based on measured correlations between wind and a solid wave surface having an ocean-like three-dimensional surface topography. Fundamental differences are found between the different wind components. The measurements suggest a quasipotential description of the wave perturbation of the flow, and the model is built on such an analysis.

The results are shown to be close to what has been found by others for situations where there is a significant gap between the wave velocity and the wind velocity. Further studies, using both spatial coordinates and the temporal coordinate t as parameters, would be instructive to improve modeling in situations where this condition is not satisfied.

Acknowledgment

This work was sponsored by Kongsberg Aerospace through the New Anti-Ship Missile Program.

References

[1] Arya, S. P., "Atmospheric Boundary Layers over Homogenous Terrain," *Engineering Meteorology*, edited by E. Plate, Elsevier, Amsterdam, 1982, pp. 233–267.

[2] Kitaigorodskii, S. A., "Influence of Surface Sea Waves on the Turbulent Regime in the Lower Part of the Marine Surface Layer of the Atmosphere," *The Physics of Air-Sea Interaction*, Israel Program for Scientific Translations, Jerusalem, 1973, Chap. 3 (translated from Russian).

[3] Antonia, R. A., and Chambers, A. J., "Wind-Wave-Induced Disturbances in the Marine Surface Layer," *Journal of Physical Oceanography*, Vol. 10, April 1980, pp. 611–622.

[4] Hristov, T. S., Friehe, C. A., Miller, S. D., Edson, J., and Wetzel, S., "Structure in the Atmospheric Surface Layer over Open Ocean Waves: Representation in Terms of Phase Averages," *Wind-Over-Wave Couplings: Perspectives and Prospects*, Inst. of Mathematics and Its Applications, Southend-on-Sea, Essex, England, UK (to be published).

[5] Mastenbroek, C., Makin, V. K., Garat, M. H., and Giovanangeli, J. P., "Experimental Evidence of the Rapid Distortion of Turbulence in the Air Flow over Water Waves," *Journal of Fluid Mechanics*, Vol. 318, July 1996, pp. 273–302.

[6] Elder, F. C., Harris, D. L., and Taylor, A., "Some Evidence of Organized Flow over Natural Waves," *Boundary-Layer Meteorology*, Vol. 1, No. 1, 1970, pp. 80–87.

[7] Lesieutre, D. J., Nixon, D., Dillenius, M. F. E., and Torres, T. O., "Analysis of Missiles Flying Low over Various Sea States," AIAA Paper 90-2855, Aug. 1990.

[8] Venås, B., and Sætran, L. R., "Simulations of Wind Along Flight Trajectories in the Ocean Surface Layer," *Journal of Aircraft*, Vol. 35, No. 2, 1998, pp. 169–174.

[9] Bowden, K. F., *Physical Oceanography of Coastal Waters*, Ellis Horwood, Chicester, England, UK, 1983, Chaps. 3 and 4.

[10] Kondo, J., Fujinawa, Y., and Naito, G., "Wave-Induced Wind Fluctuations over the Sea," *Journal of Fluid Mechanics*, Vol. 51, Pt. 4, 1972, pp. 751–771.

[11] Kendall, J. M., "The Turbulent Boundary Layer over a Wall with Progressive Surface Waves," *Journal of Fluid Mechanics*, Vol. 41, Pt. 2, 1970, pp. 259–281.

[12] Hasselmann, D. E., Dunckel, M., and Ewing, J. A., "Directional Wave Spectra Observed During JONSWAP 1973," *Journal of Physical Oceanography*, Vol. 10, Aug. 1980, pp. 1264–1280.

[13] Counihan, J., "An Improved Method of Simulating an Atmospheric Boundary Layer in a Wind Tunnel," *Atmospheric Environment*, Vol. 3, No. 2, 1969, pp. 197–214.

[14] Venås, B., and Sætran, L. R., "Simulation of Wind Near a Wavy Surface," Norwegian Univ. of Science and Technology, MTF-Rept. 1996:129(c), Trondheim, Norway, April 1996 (in Norwegian).

[15] Baher, H., *Analog & Digital Signal Processing*, Wiley, New York, 1990, p. 78.

[16] Frederick, K. A., and Hanratty, T. J., "Velocity Measurements for a Nonseparated Flow over Solid Waves," *Experiments in Fluids*, Vol. 6, No. 7, 1988, pp. 477–486.

[17] Zilker, D. P., and Hanratty, T. H., "Influence of the Amplitude of a Solid Wavy Wall on a Turbulent Flow. Part 2. Separated Flows," *Journal of Fluid Mechanics*, Vol. 90, Pt. 2, 1979, pp. 257–271.

[18] Belcher, S. E., Harris, J. A., and Street, R. L., "Linear Dynamics of Wind Waves in Coupled Turbulent Air-Water Flow. Part 1. Theory," *Journal of Fluid Mechanics*, Vol. 271, July 1994, pp. 119–151.

[19] Belcher, S. E., Newley, T. M. J., and Hunt, J. C. R., "The Drag on an Undulating Surface Induced by the Flow of a Turbulent Boundary Layer," *Journal of Fluid Mechanics*, Vol. 249, April 1993, pp. 557–596.

P. R. Bandyopadhyay
Associate Editor